ELSEVIER

Analyzing spatiotemporal variability of heterotrophic soil respiration at the field scale using orthogonal functions

Alexander Graf [a,*], Michael Herbst [a], Lutz Weihermüller [a], Johan A. Huisman [a], Nils Prolingheuer [a], Ludger Bornemann [b], Harry Vereecken [a]

[a] Agrosphere (IBG-3), Jülich Research Centre, 52425 Jülich, Germany
[b] Institute of Crop Science and Resource Conservation – Soil Science, Bonn, Germany

ARTICLE INFO

ABSTRACT

Soil CO_2 efflux was measured with a closed chamber system along a 180 m transect on a bare soil field characterized by a gentle slope and a gradient in soil properties at 28 days within a year. Principal component analysis (PCA) was used to extract the most important patterns (empirical orthogonal functions, EOFs) of the underlying spatiotemporal variability in CO_2 efflux. These patterns were analyzed with respect to their geostatistical properties, their relation to soil parameters obtained from laboratory analysis, and the relation of their loading time series to temporal variability of soil temperature and moisture. A particular focus was set on the analysis of the overfitting behaviour of two statistical models describing the spatiotemporal efflux variability: i) a multiple regression model using the k first EOFs of soil properties to predict the n first EOFs of efflux, which were then used to obtain a prediction of efflux on all days and points; and ii) a modified multiple regression model based on re-sorting of the EOFs based on their expected predictive power. It was demonstrated that PCA helped to separate meaningful spatial correlation patterns and unexplained variability in datasets of soil CO_2 efflux measurements. The two PCA analyses suggested that only about half of the total variance of efflux could be related to field-scale spatial variability of soil properties, while the other half was "noise" attributed to temporal fluctuations on the minute time scale and short-range spatial heterogeneity on the decimetre scale. The most important spatial pattern in CO_2 efflux was clearly related to soil moisture and the driving soil physical properties. Temperature, on the other hand, was the most important factor controlling the temporal variability of the spatial average of soil respiration.

© 2012 Elsevier B.V. All rights reserved.

1. Introduction

CO_2 efflux from the soil is one of the largest fluxes in the atmospheric greenhouse gas balance and of particular interest due to its potential positive feedback to global warming (IPCC, 2007). However, the environmental factors controlling the magnitude of CO_2 efflux remain difficult to disentangle, even though an increasing number of case studies have been published during past decades (for an overview, see e.g. Bond-Lamberty and Thomson, 2010). The reasons for this are rooted in the numerous interactions between environmental factors and CO_2 efflux, in combination with the different scales on which they vary in space and time (Briones, 2009; Davidson and Janssens, 2006; Mahecha et al., 2010; Wixon and Balser, 2009). Point measurements of soil CO_2 efflux have repeatedly been reported to exhibit a poor spatial dependence and strong variability at short distances (i.e. a high nugget effect, see Herbst et al., 2009; La Scala et al., 2000; Rochette et al., 1991; Rodeghiero and Cescatti, 2008). Consequently, correlations with expected driving variables in space appear to be low (Herbst et al., in press).

We hypothesize that the difficulty of understanding the driving factors of spatial variability of soil respiration is partly caused by short-term temporal fluctuations that inevitably occur during the acquisition of a spatial data set of soil CO_2 efflux. Recently, we showed that by repeating a survey with a sufficiently high frequency, the raw measurements can be decomposed by simple averaging procedures into estimates of the time-stable part of the spatial pattern of efflux, and fast fluctuations of area-averaged efflux (Graf et al., 2011). However, this study also reported that the spatial patterns were only stable for a few days. Often, measurements are only repeated at larger time intervals and the decomposition approach reported in Graf et al. (2011) cannot meaningfully be applied. Alternatively, underlying spatial patterns present in the entire data set can be investigated using empirical orthogonal functions (EOFs) derived by principal component analysis (PCA, cf. Korres et al., 2010; Perry and Niemann, 2008, for soil water content) or canonical correlation analysis. These EOFs can be related to explanatory variables such as the spatio-temporal variability of soil properties, including soil temperature and moisture amongst others. Unlike classical regression, which would link the spatial pattern of efflux to explanatory variables independently for each snapshot in time, PCA provides insight into the combined spatiotemporal dependencies of soil CO_2 efflux. PCA has also been shown to efficiently

* Corresponding author. Tel.: +49 2461 61 8676; fax: +49 2461 61 2518.
E-mail address: a.graf@fz-juelich.de (A. Graf).

separate noise from signal (e.g. Perry and Niemann, 2008), a property that would be of particular interest for soil CO_2 efflux datasets.

The aim of this study is to test whether PCA can be used to identify spatio-temporal patterns of soil CO_2 efflux with statistically significant relations to explanatory variables. We used measured CO_2 efflux from a bare soil with a gentle slope and a gradient in various soil properties, which serve as explanatory variables. To identify and describe returning spatial patterns in the efflux time series and the explanatory variables without redundancy, both datasets are turned into EOFs independently using PCA. Two types of regression models are considered: one for the two sets of EOFs in their original order, and one where EOFs are re-ordered according to their expected predictive power. For each regression model, performance on unknown samples as a function of the number of EOFs was determined by cross-validation.

2. Theoretical background

Consider the dependent variable $Y_{m,n}$ known for M sampling points and N measurement times. In addition, there are K explanatory variables contained in $X_{m,k}$. These explanatory variables vary in space, but are assumed to be persistent in time. Therefore, they are available at the same M sampling points, but without repetition in time. To determine to what extent Y can be explained by X, canonical correlation analysis (CCA, Hotelling, 1935) is frequently used. However, standard methods for solving CCA require that $min\{N, K\} < M$. If this is not the case, a common approach is to perform a principal component analysis (PCA, Hotelling, 1933) independently on both X and Y before further analysis (Muller, 1982). PCA transforms a set of variables into a set of new variables, called principal components (PCs) or empirical orthogonal functions (EOFs), that are linearly independent of each other. They are ordered by the portion of total variance in the original data that they explain (see appendix for more details). If N or K is larger than M, PCA reduces the number of non-zero new variables to M. Prior application of PCA on both X and Y reduces a subsequent CCA to a rotation (Muller, 1982). Often, the CCA step is omitted altogether and the prediction of Y from X is done by regression. Because the EOFs determined from X and Y are orthogonal, the regression coefficients can be independently determined by bivariate regression between each possible pair of EOFs. This intermediate approach between multiple regression and CCA (Jolliffe, 1982) is here referred to as PCA-based regression.

If the number of explanatory variables K is large compared to the number of sampling points M, there is a danger of overfitting. Adding an additional explanatory variable will always improve the ability of the model to fit the data (in-sample performance). However, overfitting has occurred when at the same time the ability of the model to predict independent data decreases (out-of-sample performance). In multiple regression, adjusted goodness-of-fit indices such as R^2_{adj} or Aikake´s information criterion are often used to estimate the optimum number of explanatory variables (e.g. Herbst et al., in press), or a significance test is performed for each candidate explanatory variable. For EOFs, a number of significance tests have been suggested. However, their results are often inconsistent (Peres-Neto et al., 2005; Perry and Niemann, 2008), may require prior knowledge of the correlation length in order not to overestimate the number of independent samples (Korres et al., 2010), and are not necessarily related to predictive power. Jolliffe (1982) summarized four examples demonstrating that predictive success, rather than explained variance, should be used to determine the EOFs to be included in PCA-based regression problems. Nevertheless, and in particular to ensure the relevance of the predicted EOFs of Y, we will report results of two significance tests for comparison. According to Peres-Neto et al. (2005), both are recommendable, but differently conservative.

The most direct, assumption-free, and intercomparable method to estimate out-of-sample performance, is cross-validation. A subset of the available data is excluded before parameter determination, and the goodness-of-fit indices are calculated between the predictions and measurements of Y in this unused subset only. A prerequisite for cross-validation is that the independent data set must be large enough to reliably determine the goodness-of-fit indices, but at the same time the data set remaining for model parameterisation must also be large enough. In case of a small number of sampling sites, this problem can be circumvented by the leave-one-out version of cross validation. One at a time, each of the M rows of X and Y are removed from the dataset, and the remaining M-1 rows are used to estimate the unknown model parameters. Then, each of the M alternative model versions is used to predict the row of Y values that was left out. Leave-one-out cross-validation enables us to quantify the effect of including each EOF of both the X and the Y set in the regression model, starting with the first EOF. As an EOF of X may describe a large portion of the variance of X, but not predict well any of the EOFs of Y (Jolliffe, 1982), we also test an approach where the EOFs of both X and Y are re-sorted according to the amount of variance in Y that they help to explain. This approach adds the strength of CCA to PCA-based regression, while avoiding its predictive weakness. CCA tends to assign strong weights to few or even one X and Y pair(s), if they are correlated considerably stronger to each other than the majority, independent of the portion of variance in Y they explain (Mishra, 2009). An intermediate solution between PCA and CCA was proposed by Mishra (2009) to solve this problem, but the application of this method is beyond the scope of this study because of the lack of a closed-form solution for this method. We performed CCA on our dataset and found that it did not improve out-of-sample performance as compared to PCA-based regression. For reasons of conciseness, CCA is not discussed further here.

3. Methods

3.1. Study site

Measurements were taken at the FLOWATCH test site (50°52'09"N, 06°27'01"E, 104.5 m a.s.l.), a 60 m by 190 m bare soil field (Graf et al., 2008; Weihermüller et al., 2007). In its longitudinal direction, the field is subject to a gentle slope and a strong gradient in coarse material content (Fig. 1). At the centre of the field, the fine texture (<2 mm) is classified as a silt loam. The climate is warm temperate, with an average air temperature of 9.9 °C and an annual precipitation of 698 mm (1961–2009, data taken from the climate station of the Forschungszentrum Jülich at a distance of 5.3 km from the test site). The two years of the experimental study were slightly warmer and wetter (2006: 11.0 °C, 723 mm; 2007: 11.1 °C, 878 mm). Historically, the field was typically ploughed annually up to a depth of 30 cm. Directly before and once during the study period, a grubber to a depth of 15 cm and a harrow were applied. With this treatment and several applications of glyphosate, weeds were controlled on the field site during our measurements.

3.2. Field measurements

Soil CO_2 efflux measurements were performed using a manual closed chamber system (LI-8100, Li-Cor, Lincoln, NE, USA; Xu et al., 2006) in intervals of one to two weeks between summer 2006 and autumn 2007. At each measurement point, a polypropylene collar of 10 cm depth and 20 cm inner diameter was permanently installed such that the upper edge protruded 2 cm above the average soil surface. Collars were kept free of plants as much as possible and were removed only for soil grubbering and harrowing. The location of each measurement point was determined using a differential GPS system (GPS-702-GG/Propak V3, NovAtel, Calgary, Alberta, Canada).

In this analysis, we use efflux data from 18 points spaced 10 m apart in a transect following the main height and stone content gradient of the field site (Fig. 1). For this transect, complete efflux records
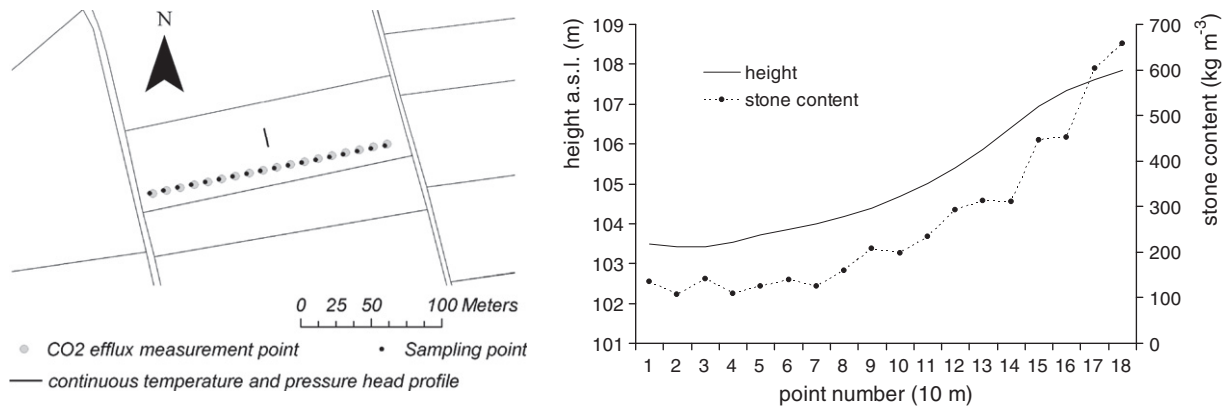
Fig. 1. Overview of the measurement site with height profile and stone content along the measurement transect.

are available for 28 days starting directly after the first grubber/harrow treatment on September 20, 2006 and ending on October 23, 2007. The chamber was placed on each collar and was closed for 2 minutes. The increase of the CO_2 concentration in the chamber headspace was measured from closing until reopening, and the measured CO_2 concentration was corrected for water vapour dilution. A one minute period between each chamber measurement was used to place the system at the next collar and to automatically purge the tubes. Soil CO_2 efflux was calculated by fitting a linear regression to the CO_2 concentration measured from 30 s after closure until reopening. From the accuracy of the individual 1 s measurements, as well as from comparing the linear fit to a less robust but more theory-based exponential fit, a resulting efflux uncertainty of about 0.1 to 0.2 µmol m^{-2} s^{-1} may be expected.

At most measurement days, additional information about soil temperature and water content were simultaneously recorded next to each collar. The measurement methodology for these state variables was changed during the study period. Until April 2007, soil water content was estimated from 3 vertical measurements with the theta probe (Delta-T, Cambridge, UK, 6 cm rod length) in the vicinity of the soil collars. Soil temperature was measured with a type E thermocouple as provided with the soil CO_2 efflux system. The thermocouple was inserted 3 cm into the soil. From June 2007 on, custom-built 3 rod TDR probes of 10 cm length were permanently installed horizontally at 8 cm depth directly below each collar. The TDR probes were connected to a TDR100 cable tester (Campbell Scientific, Logan, NE, USA) during each CO_2 measurement and water content was calculated using Topp's equation (Topp et al., 1980). To study the relation of the occurrence of patterns and spatial averages to environmental variables that vary in time, we use additional permanent measurements of soil temperature and pressure head. About 20 m north of the transect, a continuous monitoring trench is located (Fig. 1). In May 2006, 18 pF-Meters (EcoTech, Bonn, Germany) with a shaft length of 20 cm were inserted horizontally into the soil at depths of 0.15, 0.30, 0.45, 0.60, 0.90, and 1.20 m with 3 repetitions for each depth. The pF-Meters provide information about soil temperature, and pressure in a wide pressure head range. All pF-meter data were logged at 1 h intervals.

3.3. Sampling and laboratory measurements of explanatory variables

In October 2007, soil samples were taken from the field site in a 10 by 10 m grid, one row of which had its sampling points close to the CO_2 efflux transect (Fig. 1). Three auger probes were taken from the 0 to 0.30 m depth, mixed, sieved to <2 mm, and air dried. A subsample from each point was analyzed for organic carbon (C_{org}), anorganic carbon (C_{anorg}), total nitrogen (N), phosphorous (P), and calcium (Ca) at the Institute of Central Chemical Analysis (ZCH) of the Forschungszentrum Jülich. Another subsample was analyzed for grain size

distribution (wet sieving and pipette), particulate organic matter (POM, Amelung and Zech, 1999), and dithionite soluble iron oxides (dithionite citrate bi-carbonate method; Mehra and Jackson, 1960) at the Agricultural Faculty of the University of Bonn, as described by Bornemann et al. (2010). Abiotic networks of iron oxides are supposed to have a stabilizing effect on soil organic matter (Mayer et al., 2004). Thus, locations with high contents of dithionite-soluble iron might be expected to have relatively low CO_2 efflux. This would also be expected for locations with large amounts of inert black carbon and small amounts of POM, which represents the most labile carbon fraction (Herbst et al., in press). Generally, locations with a large amount of organic carbon should have the potential to release more CO_2 than locations with lower C_{org} content. The nutrients N, Ca and P might have a limiting influence on microbial growth and activity, which again could affect the microbial carbon turnover and associated CO_2 efflux. The amount of Ca will also influence soil pH.

To estimate stone content (fraction >2 mm), additional samples of 10 kg ± 5 kg were taken from the top 0.30 m. These samples were analyzed by wet sieving at the Agricultural Faculty of the University of Bonn. Finally, dry bulk density and area-averaged C and N content were determined for the CO_2 efflux measurement points themselves after removing the collars in autumn 2007. Here, each collar was used as a Kopecky ring by inserting the entire collar into the soil. Dry bulk density was calculated from the exact height and diameter of each collar and soil mass after oven drying at 60 °C for 72 h. After drying, a well-mixed subsample from each location was sieved (<2 mm) and analysed in the same way as described above for C_{org}, C_{anorg}, and N content. Stone content and dry bulk density were used to calculate the density of fine soil at each point. Multiplication of the latter with the mass fraction of each of the chemical parameters described above, resulted in its density. The slope at each position was calculated from a digital elevation model, supplied by the geological service North-Rhine Westphalia. Altogether, 19 explanatory variables are considered in our analysis (Table 1).

3.4. Data processing

An overview of the data processing procedure is given in Fig. 2, and explained in more detail below. In a first step, variables were transformed by taking their logarithm and calculating the z-score. The matrix containing these z-scores is given by:

$$_zY_{m,n} = \frac{\ln\left(efflux_{m,n}\right) - \overline{\ln\left(efflux_{1:M,n}\right)}}{\sigma\left(\ln\left(efflux_{1:M,n}\right)\right)} \tag{1}$$

where the indices m and n indicate the running number of the measurement point and measurement date, respectively. The overbar

Table 1

Explanatory variables from soil sampling and consecutive laboratory analysis. Column "ln?" indicates whether the variable was log-transformed or not, depending on the skewness reduction criterion.

Name	Units	Sample	Analysis	ln?
position along transect	m	GPS	FZJ(ICG4)	N
height above sea level	m	GPS	FZJ(ICG4)	Y
slope	°	DEM	Geol. Servive	N
bulk density	kg/m³	collar	FZJ(ICG4)	Y
N (nitrogen)	kg/m³	collar	FZJ(ZCH)	N
Corg (organic carbon)	kg/m³	collar	FZJ(ZCH)	N
Canorg (anorganic carbon)	kg/m³	collar	FZJ(ZCH)	N
Ca (calcium)	kg/m³	auger	FZJ(ZCH)	Y
P (phosphorous)	kg/m³	auger	FZJ(ZCH)	Y
stone content	kg/m³	spade	Univ. Bonn	Y
sand content	kg/m³	auger	Univ. Bonn	Y
silt content	kg/m³	auger	Univ. Bonn	N
clay content	kg/m³	auger	Univ. Bonn	Y
POM$_c$ (coarse particulate organic matter)	kg/m³	auger	Univ. Bonn	Y
POM$_m$ (intermediate ")	kg/m³	auger	Univ. Bonn	Y
POM$_f$ (fine ")	kg/m³	auger	Univ. Bonn	Y
$_{non}$POM (non-")	kg/m³	auger	Univ. Bonn	Y
BC (black carbon)	kg/m³	auger	Univ. Bonn	Y
FeDith (dithionite-soluble iron)	kg/m³	auger	Univ. Bonn	Y

denotes averaging of the column indicated by the indices, and σ its standard deviation. Eq. (1) was also applied to all explanatory variables X. However, the log transformation function was only applied to variables for which it reduced skewness.

In a next step, PCA was performed on the $_zX$ and $_zY$ matrix independently. Because the number of explanatory variables (K) and measurement days (N) were larger than the number of measurement points (M), only the first $M-1$ EOFs of each X and Y had nonzero entries. For every possible pair of EOFs determined from X and Y, ordinary linear regression was applied. Because the average of each EOF is zero, the intercept was also zero for the linear regression and the slope B was calculated according to:

$$B_{k,n}(EOF(_zY)EOF(_zX)) = \frac{\sum_{m=1}^{M} EOF_{m,k}(_zX)EOF_{m,n}(_zY)}{\sum_{m=1}^{M} \left[EOF_{m,k}(_zX) \right]^2}$$ (2)

Here, $EOF_{m,k}(_zX)$ was the value of the kth EOF of $_zX$ at measurement point m. The explained variance, R^2, was calculated using:

$$R^2_{k,n}(EOF(_zY)EOF(_zX)) = B_{k,n}(EOF(_zY)EOF(_zX))B_{n,k}(EOF(_zX)EOF(_zY))$$ (3)

Because of the linear independence of EOFs, the equations for multiple regression are described by the following matrix multiplication:

$$EOF_{1:M,1:N}(_zY) + \gamma_{1:M,1:N} = EOF_{1:M,1:K}(_zX) \cdot B_{1:K,1:N}(EOF(_zX)EOF(_zY))$$ (4)

The prediction error γ vanishes if we use all M available nonzero EOFs of X to predict the EOFs of Y. Since such a model would be strongly overfitted, it is more appropriate to not consider all EOFs of X, i.e. replacing their entries by zeroes before applying Eq. (4). In order to confine the number of possible models, we first sort the EOFs and then consider only the first k EOFs, with $k = 1 \ldots M$. Two ways to sort the explanatory EOFs are tested. First, the EOFs were sorted according to the explained variance as directly provided by the PCA. However, early EOFs may be unimportant, and later EOFs important, when it comes to predicting another variable (Jolliffe, 1982). Therefore, we tested a second approach in which the explanatory EOFs were sorted using a criterion that is related to explained variance in the dependent EOFs. For this criterion, we construct a matrix C with entries for each pair of explanatory and dependent EOF:

$$C_{k,n} = R^2_{k,n}\left(EOF(_zY)EOF(_zX)\right) \cdot \sigma^2 \left(EOF_{1:M,n}(_zY)\right)$$ (5)

where $R^2_{k,n}(EOF(_zY)EOF(_zX))$ is the proportion of variance in the nth $EOF(_zY)$ explained by the kth $EOF(_zX)$ as given by Eq. (3). The element-wise multiplication with the total variance in $_zY$ explained by the nth $EOF(_zY)$ as given by Eq. (A3) yields the amount of variance in $_zY$ that can be explained by the kth $EOF(_zX)$ via the nth $EOF(_zY)$. The sum of all entries in row k of C is the maximum amount of variance in $_zY$ that can be explained by the kth $EOF(_zX)$, if all $N\,EOF(_zY)$ are used to estimate $_zY$.

However, not only EOFs of $_zX$ may cause overfitting. In an analogous manner, trying to predict the later EOFs of $_zY$ likely means trying to predict noise. Therefore, we also consider models where only the first EOFs of $_zY$ are used to reconstruct $_zY$, while keeping measured efflux as the target variable from which all model performance indicators are
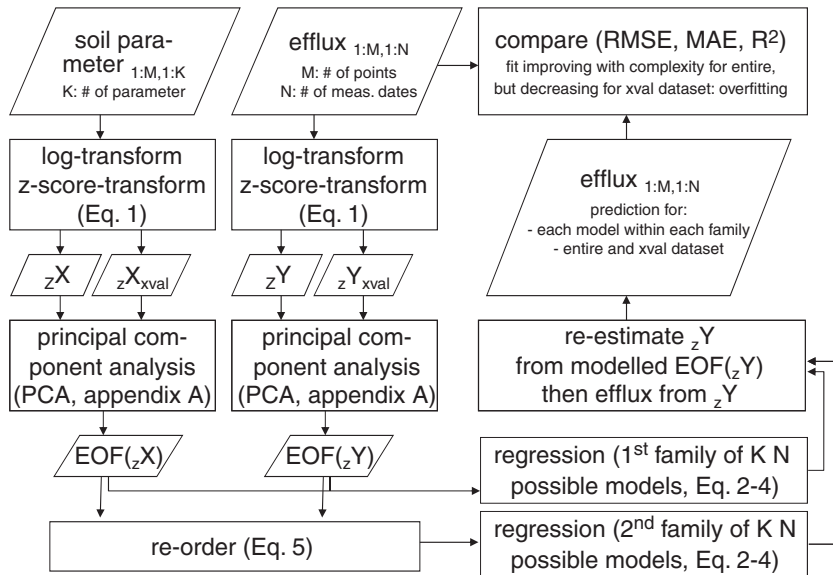
Fig. 2. Flowchart of the data processing procedure. Straight rectangles indicate processes, rhomboids datasets. "xval" indicates leave-one-out cross validation where each of the M points was removed once from the entire dataset, and soil parameters of this point have been used to estimate its efflux. "min" indicates min{K,N}. If M<K or M<N, the respective number is replaced by M when calculating the number of possible models.

calculated for intercomparability reasons. Again, either the EOF order resulting from the PCA can be used, or the sorting can be based on the matrix C, this time considering N column sums. In summary, this means inserting a version of Eq. (4) where only a part of the EOFs of $_zX$ are used, into the analogous Eq. (A4) for $_zY$. If we further replace the two EOF matrices of $_zX$ and $_zY$ according to Eq. (A2), it becomes obvious that EOF-based regression can be written in a single model equation, which resembles a multiple regression equation that includes all explanatory variables. In multiple regression, overfitting is avoided by not considering variables that do not explain variability. In the case of EOF-based regression, all explanatory variables are always included, but the regression coefficients change whenever an EOF of $_zY$ or $_zX$ is not considered:

$$_zY_{1:M,1:N} + \mu_{1:M,1:N}(k,n) = {_zX_{1:M,1:K}} \cdot E_{1:K,1:k}\left(R_{1:K,1:K}(XX)\right)$$
$$\cdot B_{1:k,1:n}(EOF(_zY)EOF(_zX)) \cdot \left[E_{1:K,1:n}\left(R_{1:N,1:N}(YY)\right)\right]' \qquad (6)$$

The prediction error μ decreases when the number of EOFs of $_zX$ and $_zY$ used to reconstruct Y increases, but at the same time the risk of overfitting increases. In order to find a balance, we applied Eq. (6) in its $K N$ different forms to M cross-validation datasets in which one measurement point has been left out. The models thus obtained were used to predict the efflux from the left-out point, including the back-transformation of Eq. (1) before any error was calculated. As we aimed to treat efflux from the respective point as truly unknown, the average and standard deviation for this back-transformation were estimated without considering the point that was left out. To see whether even the simplest model with k and $n = 1$ is an improvement with respect to the mean daily efflux, we included an estimate from this mean as case $k = 0 \mid n = 0$. The whole test run through k and n was done for the classic EOFs and the re-sorted EOFs using the C criterion.

4. Results and discussion

4.1. Efflux EOFs and their univariate properties

The efflux dataset is characterized by an average efflux of $1.57 \, \mu\text{mol m}^{-2} \, \text{s}^{-1}$, with a maximum of 6.02 and a minimum of $0.13 \, \mu\text{mol m}^{-2} \, \text{s}^{-1}$. The total standard deviation is $1.00 \, \mu\text{mol m}^{-2} \, \text{s}^{-1}$, and the temporal standard deviation of spatially averaged efflux ($0.65 \, \mu\text{mol m}^{-2} \, \text{s}^{-1}$) is in a similar order of magnitude as the spatial standard deviation of point averages ($0.97 \, \mu\text{mol m}^{-2} \, \text{s}^{-1}$). The whole dataset has a positive skewness of 1.4 and a high (traditional) kurtosis of 5.79, which reduces to near-normal values of -0.6 and 3.4 after log-transformation.

Fig. 3 shows example semivariograms from six different measurement days for the log- and z-transformed efflux data, $_zY$ before the PCA analysis. The model semivariogram is based on the nonlinear least squares Matérn family fitting routine described by Minasny and McBratney (2005). The first case (example type I) is the variogram model with the best fit ($R^2 = 0.97$) in the whole dataset. Each subpanel is roughly representative of one of six variogram types that occurred repeatedly. The first four types differ in boundedness (visibility of correlation length, upper/lower subpanel row) and quality of the model fit (left/right subpanel columns). We found five unbounded variograms with a good variogram model fit (type I), five unbounded variograms with only a mediocre model fit (type II), five bounded variograms with a good variogram model fit (type III), two bounded variograms with a poor fit (type IV), four variograms where the semivariance decreased with increasing distance (type V), and seven variograms that hardly show spatial correlation and high scatter in the experimental variogram, which leads to poor fits of the variogram model (type VI). The majority of these variograms show high nugget effects (i.e., high fraction of variance at short

distances relative to total variance) and poor fits of the variogram model, which is in agreement with previous findings (e.g. Herbst et al., 2009; La Scala et al., 2000). Only type I and III, i.e. 10 out of 28 days, clearly show a well-defined spatial dependence.

An overview of the results of the transformation of efflux data into EOFs is given in Fig. 4. The first EOF (upper left panel) explains about one third of the total variance of the z-score of log-transformed efflux $_zY$. It mostly shows smooth changes from one point to the next, with the exception of a sharp peak at point 2. In general, EOF 1 increases towards the higher end of the site. Its loadings on $_zY$ (upper mid panel) are negative on most measurement days. It should be noted that signs of EOFs are arbitrary and may depend on the solution strategy. The first EOF and its loadings indicate that efflux typically increased towards the lower part of the field. This is in agreement with the pattern resulting from arithmetic averaging $_zY$ over all measurement days, which results in a similar, but less smooth pattern, as EOF 1 reverted (not shown). To gain further insight into the use of each EOF in empirical spatial modelling, we also calculated the semivariogram for all 28 raw data arrays and their nonzero EOFs. The first EOF yielded a variogram which indicated a strong spatial correlation with low variability at small distances (upper right panel). The estimated nugget effect is less than 10%, and the variogram model fitted the experimental variogram with a high R^2 of 0.96. Because the site has a gradient in soil properties, the semivariance of EOF 1 steadily increases and does not reach the full correlation length or sill. When the data are linearly detrended, the range (here defined as the distance where the normalized semivariance reaches 95%) would be 51 m (not shown).

The second EOF shows no clear large-scale pattern and is considerably less smooth, but a tendency towards higher variability in the lower part of the site can be observed. A feature of particular interest is the minimum observed at point 2. As EOF 2 has about the same proportion of positive and negative loadings, its value at this point counteracts the peak observed in EOF 1 on some days, while amplifying it at others. The loading time series of EOF 1 and 2 are weakly positively correlated ($r = 0.32$), indicating that the two EOFs counteracted rather than amplified each other on most days. Despite the rougher pattern, the variogram of EOF 2 shows a clear spatial dependence with a low nugget effect. However, the experimental variogram shows more scatter, resulting in a poorer model fit ($R^2 = 0.82$). In addition, the unboundedness of the experimental variogram is even more evident, as indicated by the derivative of the fitted variogram model, which still increases at 150 m. This unboundedness is also conserved when removing the linear trend. All further EOFs (3 and 4 shown as examples) have no clear spatial trend, approximately the same number of positive and negative loadings, and poor variograms. Zero variance is reached after the 17th EOF. According to the test statistic Rnd-Lambda (Peres-Neto et al., 2005), only the first EOF is significant ($p < 0.1\%$), while according to the more liberal test statistic Avg-Rnd (Peres-Neto et al., 2005), the first two EOFs are non-trivial.

The ability of PCA to condense efflux information with a clear spatial dependence into the first EOFs is in good agreement with findings of Perry and Niemann (2008) for soil moisture data. The relatively small proportion of total variance explained by the first EOFs indicates that the dataset contains a large amount of spatiotemporal fluctuations introduced by singular events or measurement errors. Examples for possibly meaningful singular events in similar datasets were detailed by Graf et al. (2011). In summary, changes in incoming solar radiation or wind may cause peaks of efflux on a temporal scale of several minutes to a few hours. Such dynamics can only be detected if measurements are made continuously. In our case, the measurement interval is several days to weeks. Therefore, such events can only be treated as unexplained sources of variability in the determined spatial pattern. Continuous manual chamber measurements on transects, as presented in Graf et al. (2011), on the other hand, can usually only be performed for a few selected days because of the large effort involved. Alternatively, multiplexed automated chamber measurements
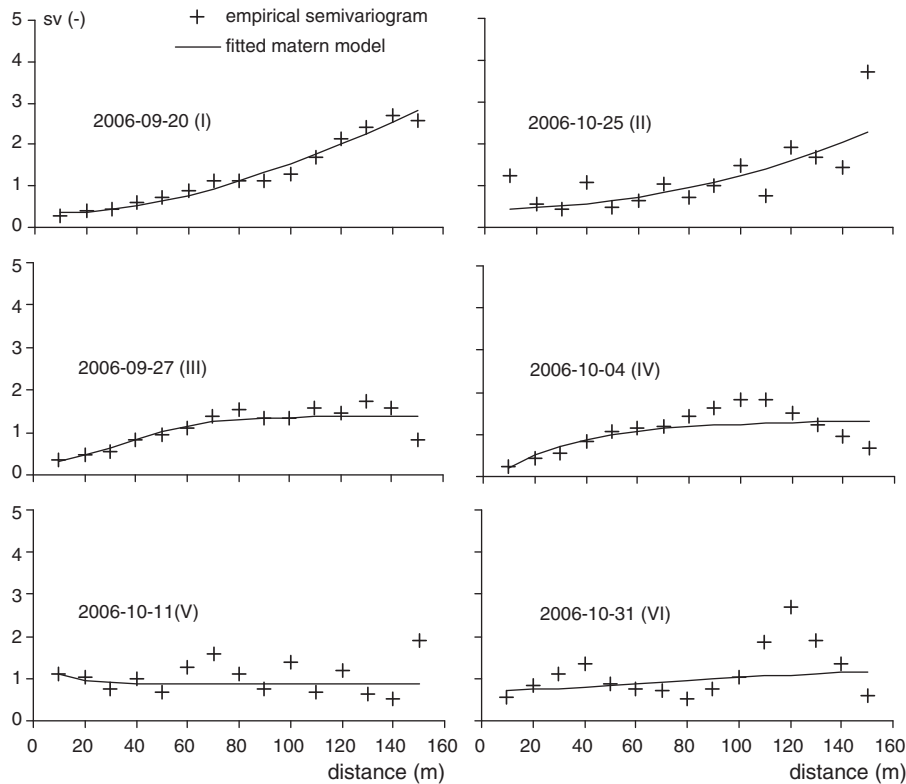
Fig. 3. Empirical semivariograms of $_zY$ on six representative days for distance bins of 10 m, and estimated Matérn models (sv: semivariance).

may produce datasets with both a high temporal resolution and a long temporal extent. However, measuring a large number of points separated by a considerable distance is a technical challenge that remains to be solved. Co-variation of efflux EOFs with temporally stable spatial variables, such as soil properties, may help to isolate meaningful spatial patterns in efflux, and will therefore be explored in the following section.

4.2. Spatial co-variability and predictability with explanatory variables

Out of the 19 explanatory variables, 13 were log-transformed due to the skewness criterion given in Section 3.4 (cf. Table 1 for details). After this, all 19 variables were z-transformed. From them, 17 non-zero EOFs were determined using PCA. As for the efflux data, the variograms of the first two EOFs showed a high spatial dependency, while the remaining EOFs showed no clear spatial correlation. The cumulative explained variance increased much faster for the EOFs of the explanatory variables than for the EOFs of the efflux data. The first two EOFs of the explanatory variables already explained 50% of the total variance. This increased to 74% when the third EOF was included, and 94% of the total variance was captured by the first six EOFs. This indicates that a limited number of underlying patterns is able to describe the explanatory variables. We attribute this small number of underlying patterns to the homogeneous site management (tillage, fertilization, and crop) and the lack of microclimatic variability (no shading or wind modification by hedges or trees). The site was selected because of its gentle slope and the associated potential for runoff, as well as for its gradient in texture caused by the variability in parent material for soil genesis (fluvial deposits from the Rhine, Meuse, and Rur River system covered by aeolian deposits). It is likely that spatial variability in any of the soil properties considered as explanatory variables is a direct or indirect effect of this gradient in texture. This is confirmed by the strongest loading of EOF 1 for stone content (-0.31). EOF 2 showed the highest negative loading for slope (-0.31), and the strongest positive loadings for several chemical

parameters, in particular for dithionite soluble iron Fe_{Dith} (0.40), total nitrogen N (0.37), calcium Ca (0.34) and coarse particular organic matter $POMc$ (0.33). According to the two significance tests already used on the efflux EOFs (Section 4.1), the first two explanatory EOFs are significant ($p < 0.1\%$).

Before analyzing the relation between explanatory and efflux EOFs in detail, it is important to first determine how many and which of the EOFs of the explanatory variables have predictive power for efflux EOFs. In order to do so, the results from the cross-validation are used to compare the in-sample and the out-of-sample performance of possible combinations of EOFs of the explanatory variables and efflux data. Fig. 5 gives the results of such a cross-validation exercise in terms of the root mean square error (*RMSE*) when the EOF order of the PCA is used.

Starting from the case $k = n = 0$, where only the average of all measurement points at a particular date is used to estimate efflux, the in-sample *RMSE* decreased with every dependent and/or explanatory EOF included in the model. At $k = n = M - 1 = 17$, the variation in efflux was completely described. The results from the cross-validation, however, indicated an improvement only with the first EOF pair, which slightly reduced the out-of-sample *RMSE* from 0.76 to 0.74 $\mu mol\ m^2\ s^{-1}$. Adding additional EOFs led to an increase of the *RMSE*. Initially, the out-of-sample *RMSE* remained stable for low k, n, but then it increased steeply to high *RMSE* values when more than 10 EOFs were used. A similar pattern is found for the mean absolute error, and a similar but reverted pattern for R^2 (not shown). This indicates that the best out-of-sample performance is obtained for using only the first explanatory EOF to predict the first EOF of the efflux data irrespective of the goodness-of-fit measure that is considered. The out-of-sample *RMSE* remained comparatively small as long as the number of EOFs from only one set (either $_zY$ or $_zX$) was increased. However, the out-of-sample *RMSE* increased steeply as soon as the number of EOFs for the explanatory variables and the efflux data were both increased simultaneously. In general, the predictive
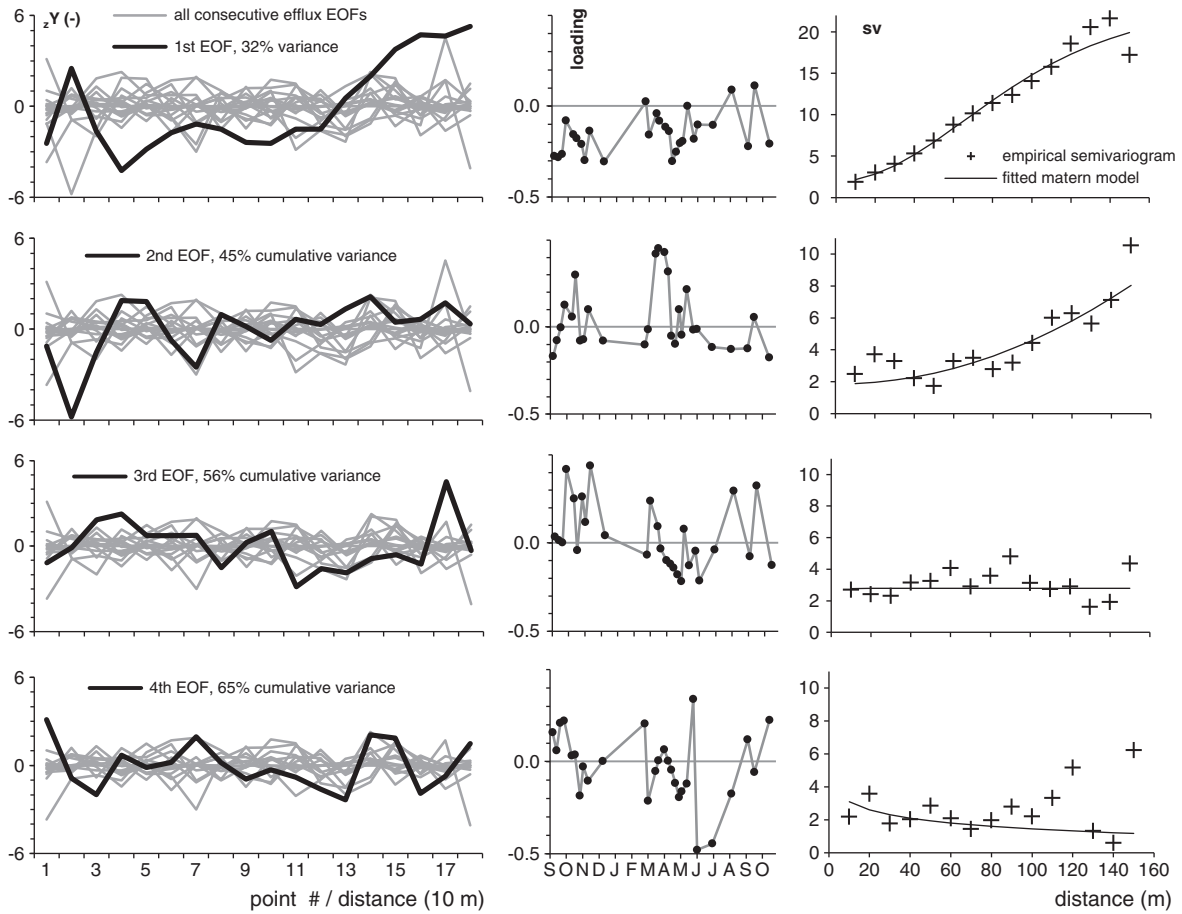
Fig. 4. Univariate properties of the first 4 EOFs calculated from the z-score of log-transformed soil CO_2 efflux $_zY$. Left column: PCA-transformed efflux per measurement point.; Middle column: Time series of the loadings on actual $_zY$ values. Right column: Empirical semivariograms for distance bins of 10 m and estimated Matérn models (sv: semivariance).

skill of the models obtained here is low, as indicated by the high out-of-sample *RMSE* and the marginal improvement of the spatial model when considering additional EOFs as compared to the predictive skill of the spatial average. This becomes particularly manifest when the lowest out-of-sample *RMSE* (0.74 µmol m^{-2} s^{-1}) is compared to the mean efflux of the whole dataset (1.57 µmol m^{-2} s^{-1}).

When re-sorting the EOFs of the explanatory variables and the efflux data according to the procedure outlined in Section 3.4, the order of the EOFs of the efflux data did not change. However, the first six EOFs of the explanatory variables did change after re-sorting (i.e. EOF 1, 3, 2, 14, 7, and 16 of the PCA analysis). The equivalent of Fig. 5c for this re-sorted set of EOFs is given in Fig. 6. As expected, the improvement of the in-sample performance with model complexity was more regular and faster in the beginning because the more predictive EOFs were now prioritized. For the out-of-sample performance, the behavior was similar although there was considerable scatter. In particular, the original explanatory EOF 3 failed to improve the prediction of unknown data points when moved to place 2. The best fit is still provided by the first pair of EOFs, which both were not affected by the resorting.

In summary, the best out-of-sample RMSE was 0.74 µmol m^{-2} s^{-1}, and the according R^2 was 0.47. On the spatial and temporal scale regarded in this study, it is not possible to provide more accurate predictions of soil CO_2 efflux from soil properties and soil CO_2 efflux measurements at neighbouring sampling locations. This result is in good agreement with a study using classical multiple regression on 61 measurements made on a single measurement day (Herbst et al., in press), where the best model had an adjusted R^2 of 0.49.

We propose two hypotheses to explain the limited predictive skill of these regression models. First, it is possible that the explanatory variables we considered do not sufficiently describe states and processes controlling spatial variability of soil CO_2 efflux at the field scale. For example, laboratory separation of meaningful carbon pools is still subject to discussion, and other space-time variants such as air filled pore space could only roughly be estimated from our dataset. However, the numerous explanatory variables we included into the analysis converged rapidly into a few EOFs, underlining the control of the stone content gradient over the other variables. Alternatively, it is possible that the measured efflux is subject to fluctuations on small temporal and spatial scales not captured in this study, or that the measurement error associated with the efflux measurements is too large. This possibility is supported by the fact that a large portion of efflux variance is related to EOFs with statistical and geostatistical properties indicating noise.

If the second hypothesis is indeed the more important part of the explanation, this may have implications for future measurement strategies beyond our site and study design. It suggests that more repetitions in time with shorter intervals are required, e.g. multiplexed automated measurements or continuous manual surveys (Graf et al., 2011). Meaningful spatial patterns could then only be extracted after averaging, or PCA analysis, of several consecutive repetitions. Alternatively, larger chambers could be used to reduce the effect of small-scale spatial variation.

A simple way to further test this hypothesis is to average efflux of three successive points, turning our measurements into a scale-filtered or aggregated dataset with less measurement points ($M = 6$). This
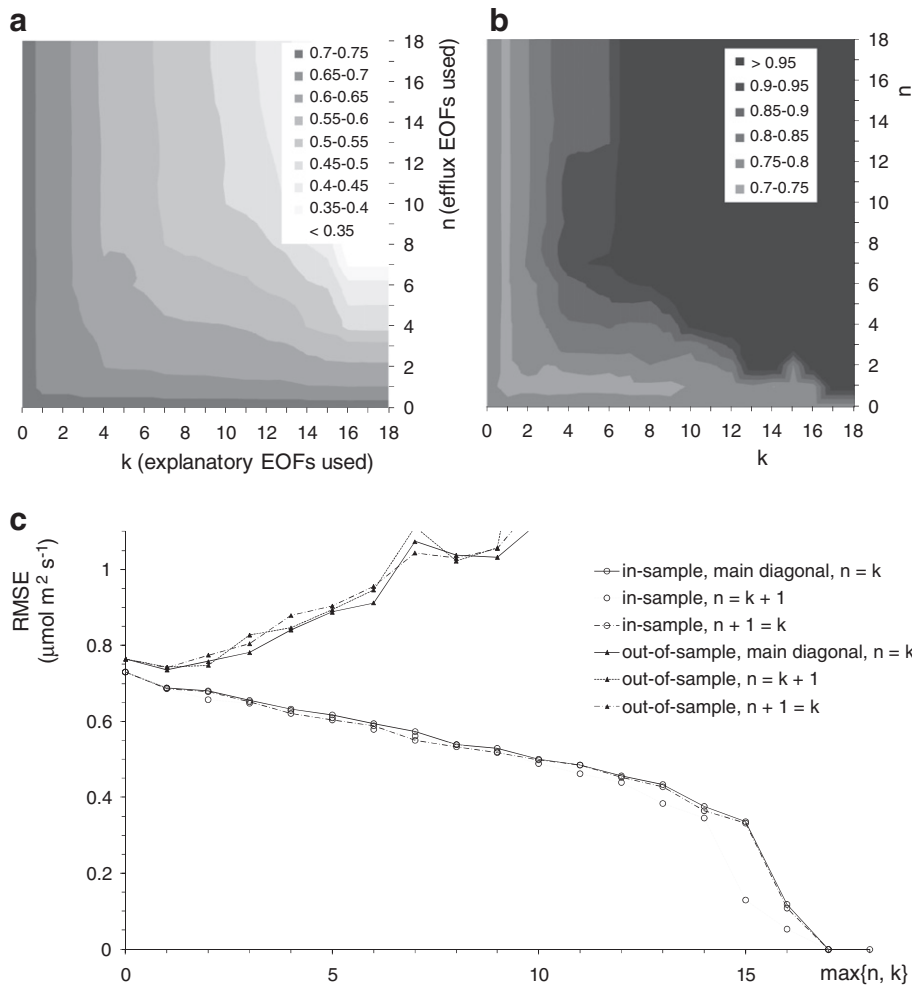
Fig. 5. In-sample and out-of-sample performance of a regression model based on EOFs of both the predicted and explanatory variables using the root mean square error (RMSE). a) RMSE (μmol m^{-2} s^{-1}) in predicting measured efflux from EOFs based on the whole dataset, as a function of the number of explanatory EOFs used for prediction and the number of dependent EOFs predicted and then used for reconstruction. b) same as a, but to predict the efflux time series at each measurement point, a version of the model is used from which this measurement point was left out. c) cross-sections through a) and b) along the main diagonal and its neighbours.

aggregation averaged out the effect of variability at scales below 30 m in space and 9 min in time. When repeating the re-sorted PCA-based regression on this dataset, the lowest out-of-sample *RMSE* improved to 0.48 μmol s^{-1} s^{-1}, and the highest out-of-sample *R²* increased to 0.67. This simple test indicates that at least a part of the problems in predicting soil CO$_2$ efflux with empirical statistical models may likely be overcome by adopting a measurement strategy with more frequent repetitions or larger chambers.

4.3. Physical interpretation and temporal variability

The out-of-sample performance of the regression models indicated that a physical meaning can only be safely assigned to spatial and temporal correlations between the first EOFs of efflux and the explanatory variables. As discussed previously, the first EOF of the efflux data is most correlated to the first EOF of the explanatory variables, which in turn mainly loads on soil physical properties. For most of the
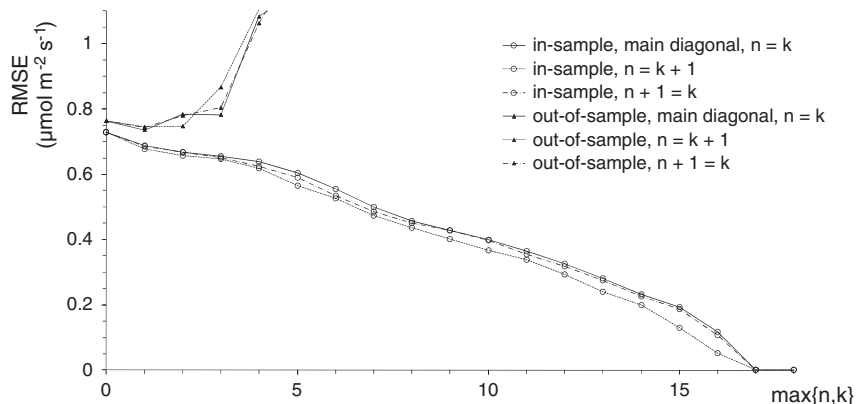
Fig. 6. Same as Fig. 5c), but for EOFs re-sorted according to Eq. (5).

measurement days, a higher efflux was obtained at locations with a lower stone content. During some days, however, this pattern was reverted. Table 2 gives an overview of this and other correlations.

The temporal variability of log-and z-transformed efflux $_zY$ is described by the loadings of its first two EOFs and its spatial average. These are related to soil temperature and pressure head at different depths in Table 2. The spatial average is highly correlated with soil temperature at all depths, but only moderately correlated with pressure head at one of the available depths. The slope of the regression of log-transformed efflux against soil temperature can be used to estimate the Q_{10} value that is commonly used to describe the temperature sensitivity of soil respiration. It was demonstrated by Pavelka et al. (2007) and Graf et al. (2008) that field-based Q_{10} values show a considerable apparent dependency on temperature measurement depth. The highest correlation between log-transformed efflux and temperature was found for a soil depth of -0.15 m (centre of historical plough layer), and the associated Q_{10} value was 2.47. The highest Q_{10} of 2.98 was found for a temperature measurement depth of -0.6 m (Fig. 7). The lowest Q_{10} value of 1.76 was found when spatially averaging all available manual surface temperature measurements.

In contrast to the spatial average of $_zY$, its first EOF is correlated with pressure head, and not significantly with temperature (Table 2). Together with the high correlation to the explanatory EOF that describes stone content, sand content and height, this indicates that the occurrence and sign of the related spatial efflux pattern is mainly controlled by soil moisture. To further test this finding, we used the manual soil water content (SWC) measurements next to each efflux point that are available for 19 of the 28 days. For each of these days, the spatial correlation is computed between $_zY$ and SWC, $R_{space}(_zY,SWC)$. It should be kept in mind that the SWC methodology changed during the course of our experiment. As long as the resulting bias is linear, however, it should not affect the correlation coefficient. We found R_{space} values between 0.74 and -0.20. Soil CO_2 efflux was spatially positively correlated to soil moisture during drier and

intermediate days (cf. Pingintha et al., 2009), and less positively or even negatively correlated during wetter days (cf. Panosso et al., 2008; Riveros-Iregui et al., 2012). The typical pattern with higher efflux from the low, fine-textured part of the transect during dry and intermediate wet days, and a lower efflux from this part of the transect on wet days, is captured by $EOF_1(_zY)$. The fact that deeper pressure head measurements were correlated more strongly to EOF 1 than the shallowest one, might be due to the temporal change of pore size distribution near the surface associated with rain compaction and soil cultivation measures. At different measurement days, the same pressure head measurement near the surface can relate to different SWCs and air-filled pore spaces. If we assume that all of these three moisture-dependent parameters, rather than a single one, affect CO_2 efflux, a measurement depth with a structure that remains stable in time is expected to better predict efflux patterns than a shallow one. Simultaneous accurate determination of pressure head, SWC and air-filled porosity in space and time, i.e. near each point at each date, might thus help to overcome a part of the low predictability problem. Unfortunately, operational measurement technology to obtain this information in situ is not available.

The same kind of spatial correlation coefficient was computed for near-surface manual temperature measurements, but no significant temporal correlation was found for this spatial correlation coefficient. We can thus conclude that temperature is the most important driver for temporal variability of area-average CO_2 efflux at our site, and that soil moisture is the most important parameter controlling spatial variation of CO_2 efflux as well as the temporal variability of this spatial pattern.

Although we expected spatial correlation between efflux and soil biochemistry parameters, this could not be conclusively confirmed in this study. The second and following EOFs from the efflux data were dominated by noise according to our cross-validation study. Nevertheless, the second EOF of the efflux data correlated to two explanatory EOFs that describe fine and coarse particular organic matter POM, phosphorous, nitrogen, and Dithionite soluble iron distribution (Table 2). However, it should be noted that this EOF has approximately as many positive as negative loadings (Fig. 3), which implies that points with a CO_2 efflux above the spatial average due to EOF 2 on some days, show a below-average efflux due to the same EOF on other days. Since we assumed that the soil properties remain relatively stable in time (and only measured them once), this supposed relationship between EOFs should be interpreted with care. It would be interesting to repeat both the soil sampling and a considerable number of efflux surveys after several years, when changes in organic matter pool composition may be expected due to the ongoing bare soil state. Any long-term change in the efflux pattern might then be related to the spatial distribution of soil organic matter stability.

5. Conclusions

We repeatedly measured soil CO_2 efflux along a transect on a bare soil with a gentle slope, and analyzed its relation to soil properties derived from surveying and sampling. Principal component analysis (PCA) was used to derive spatial patterns independently for the efflux and explanatory dataset, as well as jointly through a re-sorting algorithm. Our results indicate that:

- PCA helps to separate overall variance into patterns with well-defined geostatistical and bivariate properties and erratic patterns that represent measurement noise or fluctuations on a smaller temporal and spatial scale. This is in good agreement with results of similar studies on soil moisture (Perry and Niemann, 2008), and is to our knowledge the first such demonstration for soil CO_2 efflux. It could be particularly useful in analyzing large datasets originating from multiplexed automated chambers.
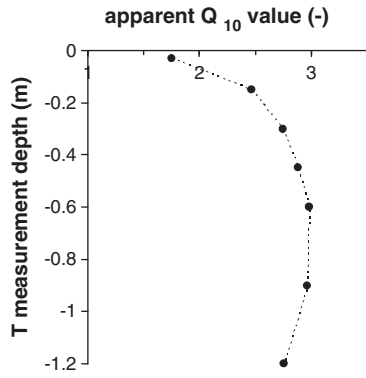
Table 2

Pearson and Spearman (bracketed) correlation coefficients between variables describing soil CO_2 efflux (columns) and spatial and temporal covariates (rows). $EOF_{n3}(_zY)$: n_3th EOF of transformed soil CO_2 efflux (spatial) and its loading on the respective date (temporal correlations). $AVG_{space}(_zY)$: Spatial average of transformed efflux. $R_{space}(_zY,SWC)$: Spatial correlation coefficient of transformed efflux with near-surface soil moisture on the respective date. T($-z$ m): Soil temperature at z m depth at monitoring station. pF ($-z$ m): log-transformed pressure head at z m depth. Sample number is 18 (M) for all spatial correlations, 19 for the temporal correlations of $R_{space}(_zY,SWC)$ and 28 (N) for all other temporal correlations. Square brackets behind each explanatory EOF indicate the variables with the most important loadings (≥ 0.3). Significance levels: *<0.05, **<0.01, ***<0.005, values with $p > 0.05$ not shown. $R_{space}(_zY,T_{soil})$ not shown due to insignificant correlations with all temporal variables.

$EOF_1(_zY)$	$EOF_2(_zY)$	$AVG_{space}(_zY)$	$R_{space}(_zY,SWC)$		
		.76(77)***		T (-0.15 m)	*correlations in time*
		.74(75)***		T (-0.30 m)	
		.73(73)***		T (-0.45 m)	
		.71(73)***		T (-0.60 m)	
	-.38*	.64(66)***		T (-0.90 m)	
	-.44*	.54(63)***		T (-1.20 m)	
				pF (-0.15 m)	
		.42*	(0.66***)	pF (-0.30 m)	
(-.46*)			.55*(61**)	pF (-0.45 m)	
-.49**(40*)			.50*	pF (-0.60 m)	
-.59(53)***			.55(51)*	pF (-0.90 m)	
-.51(48)**			.53(49)*	pF (-1.20 m)	
-0.81(68)***		$EOF_1(_zX)$ [-stone, -sand content, -height]			*in space*
	-0.49(48)*	$EOF_2(_zX)$ [Fe_{Dith}, N, POM_c, -slope]			
	-0.48*	$EOF_3(_zX)$ [C_{anorg}, -POM_f, -P]			
		$EOF_4(_zX)$			

Fig. 7. Apparent Q_{10} value (multiplication of efflux with 10 K temperature increase) as a function of temperature measurement depth. Temperature at the uppermost level –0.03 m is averaged from measurements next to each efflux point available on 22 days; all other temperatures from the automated monitoring station available on all 28 days.

- Based on cross-validation, only the first EOF of efflux was assigned a clear physical meaning. It showed significant correlation to principal components of space variables, and significant correlations of its loadings to time variables. It was not possible to increase the number of useful EOFs by modifying PCA-based regression with a re-sorting algorithm for the order of EOFs. However, this treatment produced minor improvements in the predictive skill for some later EOFs, and should be tested on further datasets.
- The spatial and temporal correlations of the first EOF of the efflux data strongly suggest that the described efflux pattern is controlled by soil moisture and soil hydraulic properties. During dry periods, points with higher soil water content produce higher efflux, while this relation is weakened or even reversed during wet periods. While soil moisture controls the spatial pattern of CO_2 efflux, the temporal variability of the area average of soil CO_2 efflux is clearly controlled by soil temperature for the climatic conditions of our site.
- More than half of the spatial variability of measured efflux is noise, caused either by the measurement process itself or fluctuations on a temporal (minutes) or spatial (decimetres) scale that cannot be described by the explanatory variables at hand. This is in agreement with another study that points at the importance of short-term fluctuations (Graf et al., 2011). A complete description of variability on all scales can thus only be achieved with many repetitions both in space and time. However, the performance improvement when modelling soil CO_2 efflux time series aggregated in space indicates that larger chamber systems may be a more efficient way to quantify field-scale variability of soil CO_2 efflux.

Appendix A. Principal component analysis (PCA)

PCA, introduced by Hotelling (1933), transforms a set of variables into principal components, also known as **EOF**s (empirical orthogonal functions) when spatial patterns are concerned (e.g. Perry and Niemann, 2008). The EOFs are linear combinations of the original variables that are orthogonal (linearly independent) to each other, with the first EOF describing as much as possible of the variance of the original dataset. PCA is described simplest if all original variables X have been transformed to their z-score $_zX$ before. As this is true for all variables in our study, we will give this simplified description here, referring the reader to the above literature for a full description.

First, the covariance between each possible pair of the K variables is computed. Due to the z-score, this covariance is identical to the Pearson correlation coefficient.

$$R_{1:K,1:K}(XX) = \frac{1}{M-1}\left[_zX_{1:M,1:K}\right]' \cdot _zX_{1:M,1:K} \qquad (A1)$$
$$\Leftrightarrow R_{k1,k2}(XX) = \frac{1}{M-1}\sum_{m=1}^{M} {}_zX_{m,k1}\,{}_zX_{m,k2}$$

The first version of Eq. (A1) is in matrix notation, which will be preferred in the following for the sake of simplicity whenever possible. The second version gives the rule for any single correlation between column k_1 and k_2. Note that throughout this appendix, X, K and k can be replaced by Y, N and n, as we use one independent PCA each on both efflux Y, and the explanatory variables X.

In a next step, the eigenvalues λ_k and eigenvectors of $R(XX)$ are determined, which is done numerically using one of the algorithms published for eigenvalue problems (in our case, the Matlab^{TM}/Octave princomp function which in turn uses the svd function). These eigenvectors are also called loadings in PCA. Matrix multiplication of $_zX$ with the eigenvector matrix E, yields a transformed version of the original data matrix, the K columns of which are the EOFs:

$$EOF_{1:M,1:K}(_zX) = {}_zX_{1:M,1:K} \cdot E_{1:K,1:K}\left(R_{1:K,1:K}(XX)\right) \qquad (A2)$$

The variance of each EOF is proportional to the corresponding eigenvalue:

$$\sigma^2\left(EOF_{1:M,k}(_zX)\right) \sim \lambda_k\left(R_{1:K,1:K}(XX)\right) \qquad (A3)$$

If normalized by the sum of all eigenvalues, this eigenvalue is also equal to the portion of variance in the original dataset that is described by the kth EOF. As mentioned above, σ_k decreases with increasing k. If $K>M$, only the first $M-1$ EOFs and their corresponding eigenvalues are nonzero. The decrease in described variance and, presumably, significant information, can be used to compose a smoothened version of the original dataset from less than K (or less than M) EOFs:

$$_zX_{1:M,1:K} + \varepsilon_{1:M,1:K}(k) = EOF_{\cdot,1:k} \cdot \left[E_{1:k,1:k}\left(R_{1:K,1:K}(XX)\right)\right]' \qquad (A4)$$

$\varepsilon(k)$ is the matrix of re-estimation errors, each entry of which depends on the number of used EOFs k, and vanishes for $k \geq min\{K,M\}$. Due to the z-score of X and the linear independence between EOFs,

the total amount of variance in $_zX$ explained by this smoothened version is equal to the sum of normalized eigenvalues of all contributing EOFs:

$$R^2\left(_zX(_zX+\varepsilon),k\right)=\frac{\sigma^2(_zX_{1:M,1:K}+\varepsilon_{1:M,1:K}(k))}{\sigma^2(_zX_{1:M,1:K})}$$

$$=\sigma^2(_zX_{1:M,1:K}+\varepsilon_{1:M,1:K}(k))=\frac{\sum_{i=1}^{k_3}\lambda_i\left(R_{1:K,1:K}(XX)\right)}{\sum_{i=1}^{K}\lambda_i\left(R_{1:K,1:K}(XX)\right)}\qquad(A5)$$

Up to this point, PCA is a standard procedure. Its continuation to an EOF-based regression is described in Section 3.4.

References

Amelung, W., Zech, W., 1999. Minimisation of organic matter disruption during particle-size fractionation of grassland epipedons. Geoderma 92, 73–85.

Bond-Lamberty, B., Thomson, A., 2010. A global database of soil respiration data. Biogeosciences 7, 1915–1926.

Bornemann, L., Welp, G., Amelung, W., 2010. Particulate organic matter at the field scale: rapid acquisition using mid-infrared spectroscopy. Soil Science Society of America Journal 74, 1147–1156.

Briones, M.J.I., 2009. Uncertainties related to the temperature sensitivity of soil carbon decomposition. Uncertainties in Environmental Modelling and Consequences for Policy Making. NATO Science for Peace and Security Series C - Environmental Security 317–335.

Davidson, E.A., Janssens, I.A., 2006. Temperature sensitivity of soil carbon decomposition and feedbacks to climate change. Nature 440, 165–173.

Graf, A., Weihermüller, L., Huisman, J.A., Herbst, M., Bauer, J., Vereecken, H., 2008. Measurement depth effects on the apparent temperature sensitivity of soil respiration in field studies. Biogeosciences 5, 1175–1188.

Graf, A., Prolingheuer, N., Schickling, A., Schmidt, M., Schneider, K., Schüttemeyer, D., Herbst, M., Huisman, J.A., Weihermüller, L., Scharnagl, B., Steenpass, C., Harms, R., Vereecken, H., 2011. Temporal downscaling of soil CO2 efflux measurements based on time-stable spatial patterns. Vadose Zone Journal 10, 239–251.

Herbst, M., Prolingheuer, N., Graf, A., Huisman, J.A., Weihermüller, L., Vanderborght, J., 2009. Characterisation and understanding of bare soil respiration spatial variability at plot scale. Vadose Zone Journal 8, 762–771.

Herbst, M., Bornemann, L., Graf, A., Welp, G., Vereecken, H., Amelung, W., in press. A geostatistical approach to the field-scale pattern of heterotrophic soil CO2 emission using covariates. Biogeochemistry. doi:10.1007/s10533-011-9661-4.

Hotelling, H., 1933. Analysis of a complex of statistical variables into principal components. Journal of Educational Psychology 24, 417–441.

Hotelling, H., 1935. The most predictable criterion. Journal of Educational Psychology 26, 139–142.

IPCC, 2007. Climate Change 2007: The physical science basis. Summary for policymakers. 18 pp.

Jolliffe, I.T., 1982. A note on the use of principal components in regression. Applied Statistics of the Journal of the Royal Statistical Society 31, 300–303.

Korres, W., Koyama, C.N., Fiener, P., Schneider, K., 2010. Analysis of surface soil moisture patterns in agricultural landscapes using Empirical Orthogonal Functions. Hydrology and Earth System Sciences 14, 751–764.

La Scala, N., Marques, J., Pereira, G.T., Cora, J.E., 2000. Short-term temporal changes in the spatial variability model of CO2 emissions from a Brazilian bare soil. Soil Biology and Biochemistry 32, 1459–1462.

Mahecha, M.D., Reichstein, M., Carvalhais, N., 2010. Global Convergence in the temperature sensitivity of respiration at ecosystem level. Science 329, 838–840.

Mayer, L.M., Schick, L.L., Hardy, K.R., Wagal, R., McCarthy, J., 2004. Organic matter in small mesopores in sediments and soils. Geochimica et Cosmochimica Acta 68, 3863–3872.

Mehra, O.P., Jackson, M.L., 1960. Iron oxide removal from soils and clays by a dithionite citrate system buffered with sodium bi-carbonate. Clays and Clay Minerals 7, 313–317.

Minasny, B., McBratney, A.B., 2005. The Matérn function as a general model for soil variograms. Geoderma 128, 192–207.

Mishra, S.K., 2009. Representation-constrained canonical correlation analysis: a hybridization of canonical correlation and principal component analyses. Munich Personal RePEc Archive 12948. http://mpra.ub.uni-muenchen.de/12948/.

Muller, K.E., 1982. Understanding canonical correlation through the general linear model and principal components. The American Statistician 36, 342–354.

Panosso, A.R., Pereira, G.T., Marques, J., La Scala, N., 2008. Variabilidade espacial da emissao de CO2 em latossolos sob cultivo de cana-de-acucar em differentes sistemas de manejo (Spatial variability of CO2 emission on oxisol soils cultivated with sugar cane under different management practices. Portuguese, with English abstract). Engenharia Agricola 28, 227–236.

Pavelka, M., Acosta, M., Marek, M.V., Kutsch, W., Janous, D., 2007. Dependence of the Q10 values on the depth of the soil temperature measuring point. Plant and Soil 292, 171–179.

Peres-Neto, P., Jackson, D.A., Somers, K.M., 2005. How many principal components? Stopping rules for determining the number of non-trivial axes revisited. Computational Statistics and Data Analysis 49, 974–997.

Perry, M.A., Niemann, J.D., 2008. Generation of soil moisture patterns at the catchment scale by EOF interpolation. Hydrology and Earth System Sciences 12, 39–53.

Pingintha, N., Leclerc, M., Beasley, J.P., Zhang, G., Senthong, C., 2009. Assessment of the soil CO2 gradient method for soil CO2 efflux measurements: comparison of six models in the calculation of the relative gas diffusion coefficient. Tellus 62B, 47–58.

Riveros-Iregui, D., McGlynn, B.L., Emanuel, R.E., Epstein, H.E., 2012. Complex terrain leads to bidirectional responses of soil respiration to inter-annual water availability. Global Change Biology 18, 749–756.

Rochette, P., Desjardins, R.L., Pattey, E., 1991. Spatial and temporal variability of soil respiration in agricultural fields. Canadian Journal of Soil Science 71, 189–196.

Rodeghiero, M., Cescatti, A., 2008. Spatial variability and optimal sampling strategy of soil respiration. Forest Ecology and Management 255, 106–112.

Topp, G.C., Davis, J.L., Annan, A.P., 1980. Electromagnetic determination of soil water content: Measurements in coaxial transmission lines. Water Resources Research 16, 574–582.

Weihermüller, L., Huisman, J.A., Herbst, M., Lambot, S., Vereecken, H., 2007. Mapping the spatial variation of soil water content at the field scale with different ground penetrating radar techniques. Journal of Hydrology 340, 205–216.

Wixon, D.L., Balser, T.C., 2009. Complexity, Climate Change and Soil Carbon: A Systems Approach to Microbial Temperature Response. Systems Research 26, 601–620.

Xu, L., Furtaw, M.D., Madsen, R.A., Garcia, R.L., Anderson, D.J., McDermitt, D.K., 2006. On maintaining pressure equilibrium between a soil CO_2 flux chamber and the ambient air. Journal of Geophysical Research 111, D08S10.